Journal of the Optical Society of America B
OPTICAL PHYSICS

Modeling the nonlinear photoabsorptive behavior during self-written waveguide formation in a photopolymer

HAOYU LI, YUE QI, RA'ED MALALLAH, AND JOHN T. SHERIDAN*

School of Electrical, Electronic and Communications Engineering, UCD Communications and Optoelectronic Research Centre, SFI-Strategic Research Cluster in Solar Energy Conversion, College of Engineering and Architecture, University College Dublin, Belfield, Dublin 4, Ireland
**Corresponding author: john.sheridan@ucd.ie*

Received 14 January 2015; revised 19 March 2015; accepted 22 March 2015; posted 25 March 2015 (Doc. ID 232595); published 27 April 2015

Photopolymer materials can be used as recording media for self-written waveguides (SWWs) as they can exhibit a large refractive index change and high photo-sensitivity. In free radical photo-polymerization systems, the dyes, functioning as the photosensitizer, strongly influence the material properties. During photo-illumination the spatial and temporal evolution of the dye concentration is an important factor leading to nonlinear absorption. In this paper, based on an investigation of the photochemical mechanisms, we analyze the nonlinear photo-absorptive effect during the photo-initiation processes. The time varying exposing light distribution is calculated and used to iteratively estimate the evolving cross-sectional refractive index and loss coefficient values. The model enables a more accurate and physical description of the optically induced growth of SWWs in such systems. Then SWWs formed in dry acrylamide/polyvinyl alcohol (AA/PVA) based photopolymer samples, containing different initial dye concentrations, are experimentally examined. The nonlinear absorptive behavior is quantified by comparing the model predictions and the experimental results.

OCIS codes: (160.5470) Polymers; (260.5950) Self-focusing; (250.5460) Polymer waveguides; (160.5335) Photosensitive materials; (130.4310) Nonlinear.

http://dx.doi.org/10.1364/JOSAB.32.000912

1. INTRODUCTION

It has been demonstrated that self-written waveguides (SWWs) can be induced in many photopolymer materials [1–10]. In this process, a writing beam gives rise to wave-guiding, which acts to focus the exposing light. Photo-polymerization, which leads to an increase of the refractive index of the medium, can cause the exposing beam to be self-trapped in the resulting optical channel [11].

Models describing the self-writing processes have been presented and applied to many types of photosensitive materials [12–15]. Generally, these phenomenological models employ two partial differential equations to describe the light propagation and the refractive index changes in response to exposure. The propagation loss is often treated as varying linearly with time, and the attenuation coefficient is treated as being constant. However, Kashin and Monro report that a nonlinear propagation loss is presented during the self-writing process [16]. This is especially true of cases involving the use of high photo-absorptive photopolymer materials. In such materials, the highly absorptive dyes which act as the photosensitizer can produce significant photo-absorptive nonlinearity. In any attempt to further develop the potential of photopolymer-based SWWs fabrication, it is necessary to include the major photo-initiation reactions taking place in the models used to describe the material behavior. This will allow a more accurate physical description of the effects of any photo-absorptive nonlinearity on the formation of SWWs in such materials.

In this paper, we describe the beam propagation loss in the material as being made up of two effects: a constant linear loss effect having a corresponding loss coefficient α_L, and a nonlinear loss effect with coefficient α_{NL}. The linear loss is regarded as being uniform; thus, the value of α_L is constant, and depends on the material intrinsic loss characteristic [17–19]. The nonlinear loss is induced by the photo-absorption process. Thus, the value of α_{NL} is determined by the spatial and temporal distribution of dye concentration within the material at any time. Experimentally, we precisely measure the time varying amount of light absorbed by a dry acrylamide/polyvinyl alcohol (AA/PVA) based photopolymer layer sensitized using different initial dye concentrations. The model developed is then used to fit the experimentally obtained results. Estimations of some of the physical parameter values appearing

in the model are found by carrying out a standard numerical fitting procedure.

This paper is organized as follows. In Section 2, the photoreactions taking place during photo-initiation are reviewed. Following a discussion of the initiation mechanisms, a set of rate equations governing the photosensitizer concentration distribution during SWWs formations is proposed. In Section 3, the predicted nonlinear absorption effects are quantitatively examined using a numerical method, i.e., the split-step Fourier method. In Section 4, the predictions of the SWWs formation simulations are presented and analyzed. In Section 5, the corresponding experimental results are presented, and the numerical predictions are fit to these results. Finally, Section 6 gives a brief conclusion.

2. PHOTOCHEMICAL ANALYSIS

During free radical photo-polymerization in materials like AA/PVA, the material is assumed to undergo four main process steps [17–22]: (1) initiation, (2) propagation, (3) termination, and (4) inhibition. In this paper, we highlight the photoreactions associated with the initiation process to examine the photo-absorptive behavior of dyes in photopolymer materials. The initiation step involves two main reactions: (1) the production of primary radicals, $R^{\bullet}$; and (2) the reaction of these primary radicals with monomer molecules to produce the chain initiating macro-radicals species [23]. To analyze the photo-absorption behavior, the process is summarized using the flow chart in Fig. 1.

When a suitable wavelength is used during exposure, the ground state dye absorbs photons ($h\nu$) and is converted into a singlet excited state, ^{1}Dye* [23] [see Eq. (1a)]. ^{1}Dye* can recover to the ground state by transfer to an electron donor (ED) molecule, or by converting back to the ground state directly by the emission of a photon by a fluorescence process [24]. ^{1}Dye* can also, in many cases, undergo intersystem crossing into a more stable and longer lived triplet state, ^{3}Dye*. ^{3}Dye* can eventually return to the ground state by radiationless transfer of a photon, or may react with the oxygen [19] to produce the singlet oxygen [20]. ^{3}Dye* may also react with the ED to produce the primary radicals ($R^{\bullet}$), and the radicalized dye (HDye$^{\bullet}$) [see Eq. (1c)]. $R^{\bullet}$ can react with the monomer to produce chain initiators, $M_1^{\bullet}$ [see Eq. (1f)]. This unstable dye can be bleached by reaction with the ED to form dihydro dye (H_2Dye) and the intermediated form of the ED (ED$_{\text{int}}$) [see Eq. (1e)]. In this paper, the two excited dye states, i.e., the singlet and triplet, are treated as being combined into one excited state, Dye*. By doing so, we avoid having to estimate the inter-crossing rate of the dye converting from singlet to the triplet, and the model is thus simplified [19–22]:

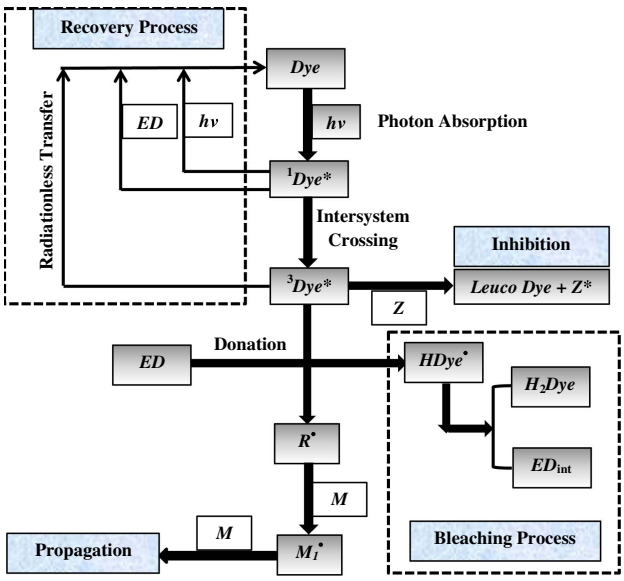

Fig. 1. Flow chart illustrating the primary photo-initiation mechanisms of a photosensitizer.

$$\text{Dye} + h\nu \xrightarrow{k_a} \text{Dye}^*, \tag{1a}$$

$$\text{Dye}^* \xrightarrow{k_r} \text{Dye}, \tag{1b}$$

$$\text{Dye}^* + \text{ED} \xrightarrow{k_d} R^{\bullet} + H\text{Dye}^{\bullet}, \tag{1c}$$

$$\text{Dye}^* + Z \xrightarrow{k_{Z,D^*}} \text{Leuco} + Z^*, \tag{1d}$$

$$\text{ED} + H\text{Dye}^{\bullet} \xrightarrow{k_b} H_2\text{Dye} + \text{ED}_{\text{int}}, \tag{1e}$$

$$R^{\bullet} + M \xrightarrow{k_i} M_1^{\bullet}. \tag{1f}$$

In Eq. (1), k_a (s^{-1}) is the rate of photon absorption by the ground state dye; k_r (s^{-1}) is the rate constant of recovery of the excited state dye back to ground state; k_d (cm^3 mol^{-1} s^{-1}) and k_b (cm^3 mol^{-1} s^{-1}) are the rate constants of dissociation of the initiator and the bleaching process, respectively; k_i (cm^3 mol^{-1} s^{-1}) is the chain initiation kinetic constant; and k_{Z,D^*} (cm^3 mol^{-1} s^{-1}) is the rate constant of inhibition of excited dye. The inhibition process is of considerable practical significance as no polymerization will take place until almost all the inhibitor is used up. Therefore, the inhibitor can act to provide a minimum exposure threshold in the material [22].

In this analysis, SWWs are assumed to be dynamically induced in the bulk samples. First, let us consider a sample in the volume space (x, y, z), with the incident beam propagating along the z direction perpendicularly illuminating the x–y plane. We propose a rate equation governing the spatial and temporal evolutions of the dye concentration, based on Eqs. (1a) and (1b):

$$\begin{aligned}\frac{\partial[A(x,y,z,t)]}{\partial t} &= \frac{\partial}{\partial x}\left\{D_A(x,y,z,t)\frac{\partial[A(x,y,z,t)]}{\partial x}\right\} \\ &+ \frac{\partial}{\partial y}\left\{D_A(x,y,z,t)\frac{\partial[A(x,y,z,t)]}{\partial y}\right\} \\ &+ \frac{\partial}{\partial z}\left\{D_A(x,y,z,t)\frac{\partial[A(x,y,z,t)]}{\partial z}\right\} \\ &+ k_r[\text{Dye}^*(x,y,z,t)] \\ &- k_a(x,y,z,t)[A(x,y,z,t)].\end{aligned} \tag{2}$$

In Eq. (2), $[A(x, y, z, t)]$ and $[\text{Dye}^*(x, y, z, t)]$ (mol cm^{-3}) represent the concentrations of the ground and excited state dyes,

respectively. $D_A(x,y,z,t)$ (cm^2 s^{-1}) is the diffusion rate of the ground state dye. As indicated in Eq. (2) the rate of production of the excited state dye $k_a(x,y,z,t)$ (s^{-1}) is no longer a constant as reported in previous holographic studies in which the incident light is assumed to be plane waves [17–22]. The relatively slow diffusion of the large dye molecules take place over an appreciably long time [19], compared to the duration of the exposure. Therefore, it is assumed that the effects of dye diffusion are negligible, i.e., $D_A(x,y,z,t) = 0$. It has been verified that the rate of removal or destruction of the photosensitizer is much faster than the recovery rate [17,18]. Thus, during exposure, dye recovery can be assumed to be negligible, i.e., $k_r \approx 0$. Therefore, Eq. (2) simplifies to

$$\frac{\partial[A(x,y,z,t)]}{\partial t} = -k_a(x,y,z,t)[A(x,y,z,t)]. \tag{3}$$

In this analysis, $k_a(x,y,z,t)$ is related to the distribution of the local illumination intensity $I(x,y,z,t)$ (mW cm^{-2}). To clarify the relationship between $k_a(x,y,z,t)$ and $I(x,y,z,t)$, a parameter Ψ_a (mol Einstein^{-1}) is introduced in this paper. We assumed that during the exposure a constant Ψ_a relates the quantum absorption efficiency of the dye and the incident local illumination intensity. Therefore, $k_a(x,y,z,t)$ is defined as

$$k_a(x,y,z,t) = \varepsilon_D \Psi_a I'(x,y,z,t), \tag{4}$$

where ε_D (cm^2 mol^{-1}) is the molar absorptivity coefficient of the dye, and $I'(x,y,z,t)$ is the light intensity converted into unit of Einstein cm^{-2} s^{-1}, as follows:

$$I'(x,y,z,t) = \frac{\lambda}{N_m hc} I(x,y,z,t). \tag{5}$$

In Eq. (5), $I(x,y,z,t)$ (mW cm^{-2}) is the local instantaneous illumination intensity, λ (nm) is the wavelength of the exposing in free space, $N_m = 6.02 \times 10^{23}$ is Avogadro's number, c (ms^{-1}) is the speed of light in free space, and h (J s) is Plank's constant. The local light intensity is defined as $I(x,y,z,t) = |E(x,y,z,t)|^2$ (mW cm^{-2}), where the amplitude of the electric field $E(x,y,z,t)$ is the solution of the paraxial wave equation [10,13–16,25] discussed in Section 3.

3. THEORETICAL ANALYSIS

A. Model Development

To predict SWWs formation, numerical simulations must be performed. When modeling self-writing in the bulk sample, the material properties (refractive index and absorptivity) are initially considered as being homogenous. The electric field of the incident beam is taken to be linearly polarized and monochromatic with angular frequency ω [25], i.e.,

$$\boldsymbol{E}(x,y,z,t) = E(x,y,z,t)\hat{\boldsymbol{x}}\ \exp[i(n_0 k_0 z - \omega t)], \tag{6}$$

where $E(x,y,z,t)$ is the amplitude of the electric field, z is the light propagation direction, x and y are the transverse coordinates, and t is the time. The initial average refractive index of the homogenous medium is n_0 and the wave number in free space is $k_0 = 2\pi/\lambda$. The light is assumed to be linearly polarized in the x-direction. Within the material light propagation is governed by the wave equation [15,26]

$$\nabla^2 \boldsymbol{E} + (k_0^2 n^2 + i\omega\mu\sigma)\boldsymbol{E} = 0, \tag{7}$$

where $\nabla^2 = \partial^2/\partial x^2 + \partial^2/\partial y^2 + \partial^2/\partial z^2$ is the 3-D Laplace operator. $n = n_0 + \Delta n$ is the current refractive index, where Δn is the change in the refractive index produced by exposure. μ is the permeability of the medium typically assumed to be that of free space, i.e., $\mu = 1$. σ is the conductivity, which is used to define the absorption parameter, $\alpha = \mu c\sigma/n_0$. Substituting Eq. (6) into Eq. (7) we obtain

$$\frac{\partial^2 E}{\partial z^2} + 2ik_0 n_0 \frac{\partial E}{\partial z} + \nabla_\perp^2 E + 2k_0^2 n_0 \Delta n E + 2k_0^2 \Delta n^2 E + ik_0 n_0 \alpha E = 0, \tag{8}$$

where $\nabla_\perp^2 = \partial^2/\partial x^2 + \partial^2/\partial y^2$ is the 2-D Laplace operator. It is known that the refractive index change Δn induced during the self-writing process are small comparing to the value of n_0 [2,4,10,12–14]. In addition, it can be assumed that the high order derivatives of the electric field can be neglected (the energy varies slowly with z). Therefore,

$$2k_0^2 n_0 \Delta n E \gg 2k_0^2 \Delta n^2 E; \quad \text{and} \quad \frac{\partial^2 E}{\partial z^2} \approx 0. \tag{9}$$

Applying these conditions gives the governing paraxial wave equation Eq. (8) [13–16]:

$$\frac{\partial E}{\partial z} = \frac{i}{2k_0 n_0}\nabla_\perp^2 E + ik_0 \Delta n E - \frac{1}{2}\alpha E. \tag{10}$$

In Eq. (10), both the index change and the attenuation parameter are assumed to vary temporally and spatially, i.e., $\Delta n(x,y,z,t)$ and $\alpha(x,y,z,t)$. As stated in Section 2, we assumed that $\alpha(x,y,z,t)$ (cm^{-1}), which governs the light loss, can be considered the sum of a constant linear loss coefficient α_L(cm^{-1}), and a nonlinear loss coefficient $\alpha_{\mathrm{NL}}(x,y,z,t)$ (cm^{-1}), i.e., $\alpha(x,y,z,t) = \alpha_L + \alpha_{\mathrm{NL}}(x,y,z,t)$. Generally, the linear loss is regarded as uniform and the value of α_L is assumed constant [17–19]. However, the nonlinear loss arises because of dye absorption and is related to the characteristics of the dye used, i.e., its concentration and molar absorptive capacity. Thus, the value of $\alpha_{\mathrm{NL}}(x,y,z,t)$ depends on the spatial and temporal distribution of $[A(x,y,z,t)]$ and the molar absorptivity coefficient of the dye, ε_D (cm^2 mol^{-1}) [15],

$$\alpha_{\mathrm{NL}}(x,y,z,t) = \varepsilon_D[A(x,y,z,t)], \tag{11}$$

$[A(x,y,z,t)]$ can be obtained by solving Eq. (3). Then the total attenuation parameter $\alpha(x,y,z,t)$ in Eq. (10) is given by

$$\alpha(x,y,z,t) = \alpha_L + \varepsilon_D[A(x,y,z,t)]. \tag{12}$$

The refractive index change induced during the self-writing process is typically described in the literature using a simple approximate phenomenological model [12–14]:

$$\frac{\partial \Delta n(x,y,z,t)}{\partial t} = A_s I(x,y,z,t)^p \left(1 - \frac{\Delta n(x,y,z,t)}{\Delta n_s}\right), \tag{13}$$

where t is the exposure time, Δn_s is the fixed saturation value of the refractive index change, and $I(x,y,z,t) = |E(x,y,z,t)|^2$ is the local light intensity [12–14]. p is the number of photons involved in the process and, for photo-polymerization, it is typically assumed to be $p = 1$ [13]. The coefficient A_s is a real coefficient that depends on the material properties, the value of p, and the wavelength of the exposure light [13,16]. It is

clear that Eq. (13) is an approximate model, which is not derived based on a physical description of the polymerization processes. In free radical photo-polymerization systems, an accurate model of the photopolymer materials should involve calculating the component concentrations using the related kinetic equations. $\Delta n(x, y, z, t)$ would then be calculated using the Lorentz–Lorenz formula [27]. However, the phenomenological model [12–14] is used because it is simple and the numerical predictions have been shown to agree reasonably well with the experimental results [10].

B. Numerical Algorithm

Eq. (10) is a nonlinear partial differential equation, and analytic solutions are only available for very specific cases [28]. Therefore, numerical methods are necessary. The algorithms used can be classified into two categories, i.e., finite-difference [29–31] and pseudo-spectral methods [32–34]. Generally, the pseudo-spectral methods achieve the same accuracy considerably faster, i.e., by up to an order of magnitude [35]. We begin by reviewing the use of a pseudo-spectral method, the *split-step Fourier method* [28], which is the main algorithm applied in our calculations. By including the time varying material properties presented in Eqs. (12) and (13), the split-step Fourier method is appropriately modified and then applied to solve the light propagation problem in nonlinear photopolymer media. To apply the split-step Fourier method, it is useful to define two operators: $\hat{D}$ a differential operator which denotes the dispersion of the light propagation, and second, $\hat{N}$ a nonlinear operator that governs the effects of material nonlinearities, i.e., nonlinear modulation induced by refractive index change and nonlinear absorption induced by dye concentration change. These operators are defined as follows:

$$\hat{D}(x, y) = \frac{i}{2k_0 n_0}\nabla_{\perp}^2, \tag{14a}$$

$$\hat{N}(x, y, z, t) = ik_0\Delta n(x, y, z, t) - \frac{1}{2}\alpha(x, y, z, t). \tag{14b}$$

Values for $\alpha(x, y, z, t)$ and $\Delta n(x, y, z, t)$ are obtained using Eqs. (12) and (13), respectively. Using these two operators, the paraxial wave equation, i.e., Eq. (10), can be rewritten as

$$\frac{\partial E(x, y, z, t)}{\partial z} = [\hat{D}(x, y) + \hat{N}(x, y, z, t)]E(x, y, z, t). \tag{15}$$

By introducing these two operators and rewriting the nonlinear partial differential equation, Eq. (10), in the form of Eq. (15), the resulting formally exact solution can be found:

$$E(x, y, z, t) = E_0(x, y, t)\exp\{z[\hat{D}(x, y) + \hat{N}(x, y, z, t)]\}, \tag{16}$$

where $E_0(x, y, t)$ is constant in z. Let us assume the field propagates a small distance Δz. Using Eq. (16) we can write that

$$E(x, y, z + \Delta z, t) = \exp\{\Delta z[\hat{D}(x, y) + \hat{N}(x, y, z, t)]\}E(x, y, z, t). \tag{17}$$

In general, dispersion and nonlinearities act simultaneously along the light propagation z-axis. However over a small step Δz, the instantaneous dispersive and nonlinear effects can be considered to be independent of z. At this point, it is useful to introduce the Baker–Hausdorff formula [36,37] for two such operators:

$$\exp(\Delta z\hat{D})\exp(\Delta z\hat{N}) = \exp\left(\Delta z\left\{\hat{D} + \hat{N} + \frac{1}{2}[\hat{D}, \hat{N}] + \frac{1}{12}[\hat{D}, [\hat{D}, \hat{N}]] - \frac{1}{12}[\hat{N}, [\hat{D}, \hat{N}]] + \cdots\right\}\right), \tag{18a}$$

where the square bracket notation is defined so that

$$[\hat{D}, \hat{N}] = \hat{D}\hat{N} - \hat{N}\hat{D}. \tag{18b}$$

In applying the split-step Fourier method, the noncommutating nature of the operators $\hat{D}$ and $\hat{N}$ is assumed to be ignored [36,37]. Thus Eq. (18a) can be approximated using

$$\exp\{\Delta z[\hat{D}(x, y) + \hat{N}(x, y, z)]\} \approx \exp[\Delta z\hat{D}(x, y)]\exp[\Delta z\hat{N}(x, y, z, t)]. \tag{19}$$

Substitute the resulting Eq. (19) into Eq. (17), the electric field in going from z to $z + \Delta z$ can be approximated by

$$E(x, y, z + \Delta z, t) \approx \exp[\Delta z\hat{D}(x, y)]\exp[\Delta z\hat{N}(x, y, z, t)]E(x, y, z, t). \tag{20}$$

From Eq. (20), it can be seen that the propagation from z to $z + \Delta z$, can be carried out in two steps. In the first step, the nonlinear operator acts, i.e., $\exp[z\hat{N}(x, y, z, t)]E(x, y, z, t)$. Then, the dispersion operator acts, i.e., $\exp[z\hat{D}(x, y)]\{\exp[z\hat{N}(x, y, z, t)]E(x, y, z, t)\}$. The exponential operator in Eq. (20) can be evaluated in the Fourier domain and shown to be equivalent to

$$\exp[\Delta z\hat{D}(x, y)]\exp[\Delta z\hat{N}(x, y, z, t)]E(x, y, z, t) = F_{x-y}^{-1}\{\exp[\Delta z\hat{D}_F(k_x, k_y)]F_{x-y}\exp[\Delta z\hat{N}(x, y, z, t)]E(x, y, z, t)\}, \tag{21}$$

where F_{x-y} denotes application of the Fourier-transform operation in the x–y plane. k_x and k_y are the corresponding spatial frequency coordinates in the Fourier domain. It should be noted that the dispersion operator appearing in Eq. (21) is in the Fourier domain (k_x, k_y), rather than in the space domain (x, y), as it is defined in Eq. (14a). Also in Eq. (21), the dispersion operator in the Fourier domain is given by

$$\hat{D}_F(k_x, k_y) = \frac{i}{2k_0 n_0}[(-ik_x)^2 + (-ik_y)^2]. \tag{22}$$

The numerical evaluation of Eq. (22) can be performed efficiently using the fast Fourier transform algorithm (FFT) [38,39]. Therefore, from Eqs. (20) and (21), it is known that the propagation of the electric field, i.e., from $E(x, y, z, t)$ to $E(x, y, z + \Delta z, t)$, can be calculated either in the Fourier domain or in the space domain:

$$E(x,y,z+\Delta z,t)$$
$$=\exp[\Delta z\hat{D}(x,y)]\exp[\Delta z\hat{N}(x,y,z,t)]E(x,y,z,t)$$
$$=F_{x-y}^{-1}(\exp[\Delta z\hat{D}_F(k_x,k_y)]F_{x-y}\{\exp[\Delta z\hat{N}(x,y,z,t)]\}E(x,y,z,t)). \quad (23)$$

In Eq. (23), the two operators are as defined in Eqs. (14b) and (22), respectively. The accuracy of the solution of Eq. (23) can be improved by adopting a different procedure [28,40] to propagate the electric field from z to $z+\Delta z$, namely by replacing Eq. (23) by Eq. (24):

$$E(x,y,z+\Delta z,t)=\exp\left[\frac{\Delta z\hat{D}(x,y)}{2}\right]\exp[\Delta z\hat{N}(x,y,z,t)]$$
$$\times\exp\left[\frac{\Delta z\hat{D}(x,y)}{2}\right]E(x,y,z,t). \quad (24)$$

The difference between Eq. (23) and (24) is that the effect of the nonlinear operator is included in the middle of the segment, rather than at the segment boundary. This scheme is known as the *symmetrized split-step Fourier method* [28,40]. In this analysis, the total thickness (in z) is d, which is split into N_z (integer) successive steps, i.e., $d=N_z\Delta z$. The electric field, as it propagates through d, is obtained using the discretized version of Eq. (24) to calculate values at every depth, i.e., at each depth of $z=l\Delta z$, where l is a integer $1\le l\le N_z$,

$$E(x,y,d,t)=\exp\left[-\frac{\Delta z\hat{D}(x,y)}{2}\right]\left\{\prod_{l=1}^{N_z}\exp[\Delta z\hat{D}(x,y)]\right.$$
$$\left.\times\exp[\Delta z\hat{N}(x,y,l\Delta z,t)]\right\}$$
$$\times\exp\left[\frac{\Delta z\hat{D}(x,y)}{2}\right]E(x,y,0,t). \quad (25)$$

In Eq. (25) $E(x,y,0,t)$ denotes the initial electric field at the input face ($z=0$).

4. SIMULATION RESULTS

The predictions of the model presented in Section 3 are now discussed. We consider a Gaussian beam propagating along z, of wavelength λ, and beam width a (at $z=0$). The maximum light intensity is $I_0=|E_0|^2$, where E_0 is the characteristic electric field amplitude. The relationship between the light power, P_0, and the maximum light intensity, I_0, is $P_0=\pi I_0 a^2$. The waist of this Gaussian beam is assumed to illuminate the bulk photopolymer material from the left at the input face ($z=0$), where the input electric field is [13,14]

$$E(x,y,0,t)=E_0\exp\left(-\frac{x^2+y^2}{a^2}\right). \quad (26)$$

Under this initial condition, we note that the pattern of the light is a centro-symmetric circle. Since all reactions taking place in the material will be similarly symmetric, to simplify the calculations, it is assumed sufficient to include only the transverse coordinate of one-dimensional (x or y), rather than performing the corresponding full two-dimensional calculations (in x and y).

To begin, a set of reasonable initial conditions must be chosen. The molar absorptivity coefficient of the dye Phloxine B (PB:$C_{20}H_2Br_4Cl_4Na_2O_5$) is $\varepsilon_D=0.8\times10^8$ cm^2 mol^{-1}, and the quantum absorption efficiency parameter is $\Psi_a=6.5\times10^{-8}$ mol Einstein^{-1} [21]. The initial physical parameter values used are: $\alpha_L=0.5$ cm^{-1}, $n_0=1.493$, $\Delta n_s=6.0\times10^{-3}$, $A_s=2.0\times10^{-12}$ cm^2 mW^{-1} s^{-1}, $a=20$ μm, $c=3\times10^8$ ms^{-1}, and $h=6.62\times10^{-34}$ Js [19]. The other parameters used for the purposes of simulation of the self-writing process are as follows: The calculation window size (in x) used is $X_W=200$ μm. The total number of points in the transverse dimension (in x) is $N_x=1000$ [38,39], and the corresponding step lengths are $\Delta x=X_W/N_x=0.2$ μm. The material thickness of the photopolymer sample used in the analysis is $d=8$ mm. The total number of steps in material normalized depth (in z) is $N_z=100$; therefore, the step length is $\Delta z=d/N_z=80$ μm. The total exposure time using a green laser source (output power $P_0=2$ mW and wavelength $\lambda=532$ nm) is $t_{\exp}=600$ s. The number of time steps used is $N_t=600$ giving a time step duration of $\Delta t=t_{\exp}/N_t=1$ s.

To examine the model predictions, simulations are performed for two cases: (1) a lower initial photosensitizer concentration, i.e., $[A]_{\text{low}}=1.22\times10^{-7}$ mol cm^{-3}, producing a relatively weak nonlinear absorption effect; and (2) for an order of magnitude higher initial photosensitizer concentration, i.e., $[A]_{\text{high}}=12.2\times10^{-7}$ mol cm^{-3}, producing a considerably higher nonlinear absorption effect.

A. LOWER DYE CONCENTRATION SIMULATIONS

Simulations are first performed for the lower initial photosensitizer concentration ($[A]_{\text{low}}=1.22\times10^{-7}$ mol cm^{-3}). Using the model developed in Section 3, the predicted formation process results are presented in Fig. 2. The results clearly illustrate the compensation of light divergence by self-focusing because of the nonlinear response of the low-loss medium.

Figure 2 shows the simulations of the cross-sectional (x–z) normalized light intensity, i.e., $I_N=I/I_0$, where I_0 is determined by the Gaussian beam power P_0. In Figs. 2(a)–2(c), as the exposure time increases from 10 to 100 s, the incident light can be seen to initially diffract (spread) as it propagates through the homogenous material, since the weak index changes taking place do not occur instantaneously. Initially, the highest light intensity distribution peak is found at the input face $z=0$. Once self-focusing begins to take place, the induced changes in the refractive index start to compensate the light diffraction spreading. In Figs. 2(d)–2(f), for illuminating times $200\le t\le600$ s, the SWW forms and the location in z of the highest intensity moves along the propagation axis (z-axis) and the maximum peak value increases. The appearance of the so-called *primary and secondary eyes* [13,14] can be seen in Figs. 2(d)–2(f).

In Fig. 3, the evolution of the proposed attenuation parameter with time, i.e., $\alpha(x,y,z,t)$ (cm^{-1}), is presented as contour plots in x–z axis for the low initial dye concentration case. Performing simulations using the model in Section 3, $\alpha(x,y,z,t)$ is obtained using Eqs. (11) and (12). The results presented in Figs. 3(a)–3(f) clearly indicate that $\alpha(x,y,z,t)$

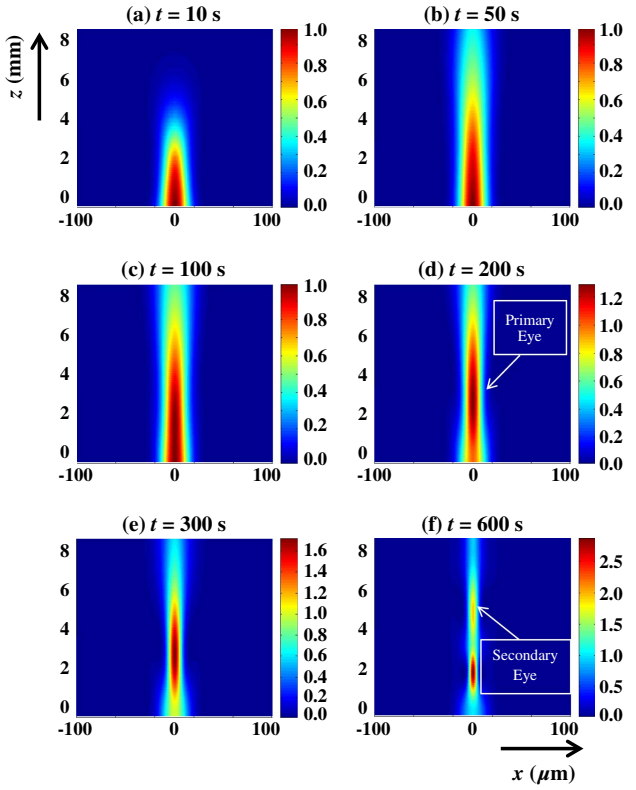

Fig. 2. Numerical predictions of the normalized light intensity distribution in x–z axis for the low dye concentration of $[A]_{low} = 1.22 \times 10^{-7}$ mol cm^{-3} case. Exposure times t = (a) 10 s, (b) 50 s, (c) 100 s, (d) 200 s, (e) 300 s, and (f) 600 s.

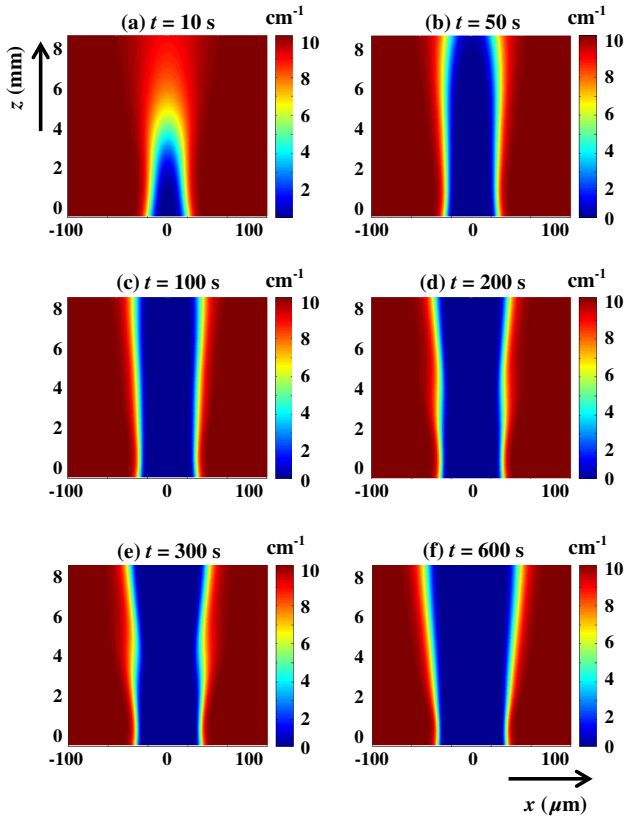

Fig. 3. Numerical simulations of $\alpha(x, y, z, t)$ (cm^{-1}) distribution in x–z axis for the low initial dye concentration of $[A]_{low} = 1.22 \times 10^{-7}$ mol cm^{-3} case. Exposure times t = (a) 10 s, (b) 50 s, (c) 100 s, (d) 200 s, (e) 300 s, and (f) 600 s.

and, thus, the absorption in the material varies with time and space and is not a constant [2,4].

To demonstrate how the evolution of the dye concentration is related to the material nonlinear absorption, the cross-sectional spatial distributions of the dye is also calculated and the predictions are shown in Fig. 4.

Examining Fig. 4(a), it can be seen that the dye is rapidly used up. The removed spatial concentration shape distorts from the exposing Gaussian beam pattern and widens into the darker surrounding regions. At greater depths, i.e., Figs. 4(b)–4(d), the consumptions of the dye concentration become less rapid, but the spatial concentration profiles clearly widen when $t \leq 60$ s. These results arise because of both the absorptive response of the photosensitizer and the initial diffraction of the incident beam. When $t = 600$ s, the dye is consumed over a wider spatial range. Dye consumption is more obvious as the depth increases, as seen in Figs. 4(c) and 4(d). However, as shown in Figs. 4(a) and 4(b), such effects are weak when $t = 600$ s. Therefore, it is predicted that the diffracted beam is primarily restrained when $z < 4$ mm because of absorption.

B. Higher Dye Concentration Simulations

Next we examine the corresponding results when a higher initial dye concentration of $[A]_{high} = 12.2 \times 10^{-7}$ mol cm^{-3} is used. As can be observed in Fig. 5, the normalized light intensity distribution exhibits two main different behaviors to those illustrated in Fig. 2. First, during exposure, the light intensity is no longer significantly present through the high loss material instantaneously. Instead, it only becomes present gradually and nonuniformly in depth. Second, as the light intensity distribution increases, its shape remains approximately constant, an effect referred to as being *self-similar* [41].

The reason for these differences is that the effects of the high absorption and self-modulation act alternately to dominate SWW formation. Initially, the effects of self-focusing are weak and not sufficient to compensate for the diffraction effects. However, most of the diffracted light is absorbed by the high concentration of active dye molecules available. Then, as the index changes are generated and the dye molecules are consumed, the diffraction effects are balanced by the self-focusing taking place. As exposure continues, this balancing process repeatedly occurs at different locations along z.

The corresponding predicted $\alpha(x, y, z, t)$ (cm^{-1}) distributions in the x–z axis are presented in Fig. 6. It should be noted that the widths of the $\alpha(x, y, z, t)$ distributions are narrower than those in Fig. 3, which is consistent with the results presented in Fig. 5.

Figure 7 shows the cross-sectional spatial variation of the dye distribution in the higher dye concentration case. Clearly, the generation of SWW is neither uniform in time or space. For example, in Fig. 7(a), the dye concentration in the exposed

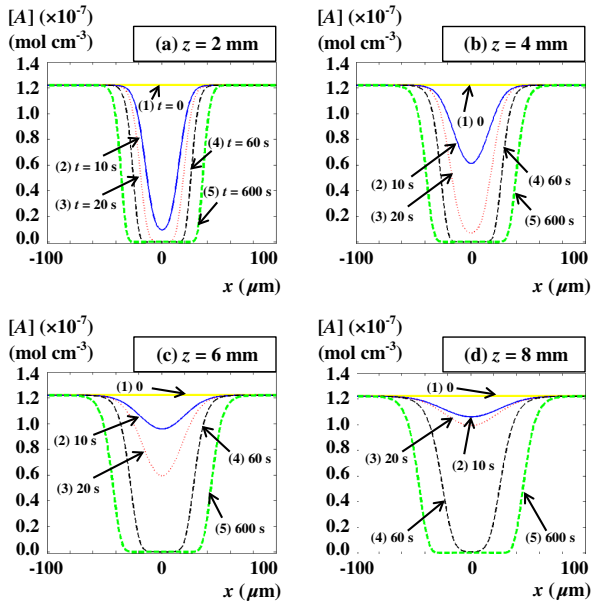

Fig. 4. Simulations of the spatial dye concentration distribution for a low initial concentration of $[A]_{low} = 1.22 \times 10^{-7}$ mol cm^{-3}, at four different material depths: z = (a) 2, (b) 4, (c) 6, and (d) 8 mm, at five different exposure times: t = (1) 0 (yellow full bold curve), (2) 10 (blue full curve), (3) 20 (red short dashed curve), (4) 60 (black long dashed curve), and (5) 600 s (green dashed bold curve).

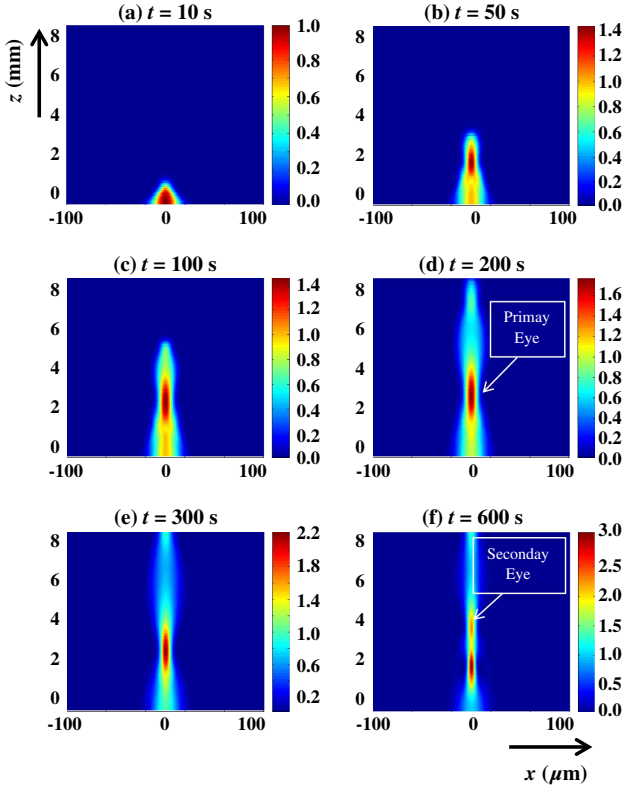

Fig. 5. Numerical simulations of normalized light intensity distribution in x–z axis for the high dye concentration of $[A]_{high} = 12.2 \times 10^{-7}$ mol cm^{-3} case. Exposure times t = (a) 10 s, (b) 50 s, (c) 100 s, (d) 200 s, (e) 300 s, and (f) 600 s.

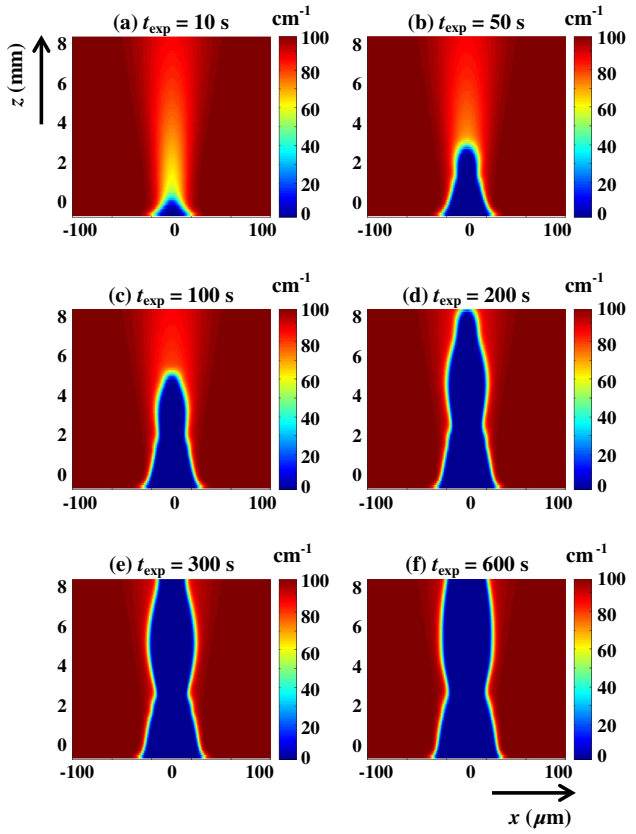

Fig. 6. Numerical simulations of $\alpha(x, y, z, t)$ (cm^{-1}) distribution in x–z axis for the high dye concentration of $[A]_{high} = 12.2 \times 10^{-7}$ mol cm^{-3}. Exposure times t = (a) 10 s, (b) 50 s, (c) 100 s, (d) 200 s, (e) 300 s, and (f) 600 s.

region is rapidly consumed in the time interval from 10 to 30 s. Between 60 and 600 s, the spatial variation of the consumed dye concentration distorts from the exposing Gaussian shape and slowly expands into the dark regions. Thus, initially most photo-absorption takes place where $z \leq 2$ mm. Then, as the dye is consumed, the light begins to expose the deeper locations. The same processes can be observed in Figs. 7(b)–7(d).

5. EXPERIMENTAL RESULTS

In this section, the predictions of the model discussed in Section 3 are compared to a range of experimental results for a standard free-radical photo-polymerization system, i.e., acrylamide/polyvinyl alcohol (AA/PVA). Preparation of the dry AA/PVA material sample used in this work has been detailed in a previous paper [10]. It is made up of five basic components: a binder (Polyvinyl Alcohol, PVA), a sensitizer dye (Phloxine B, PB), a monomer (Acrylamide, AA), a cross-linker (Bisacrylamide, BA), and an electron donor (Triethanolamine, TEA). For the specific material under examination here, the dye (Phloxine B) is used to sensitize it in the green, i.e., $\lambda = 532$ nm [42]. The experimental initial conditions, e.g., the size of samples, the input beam width and power, are as described in Section 4.

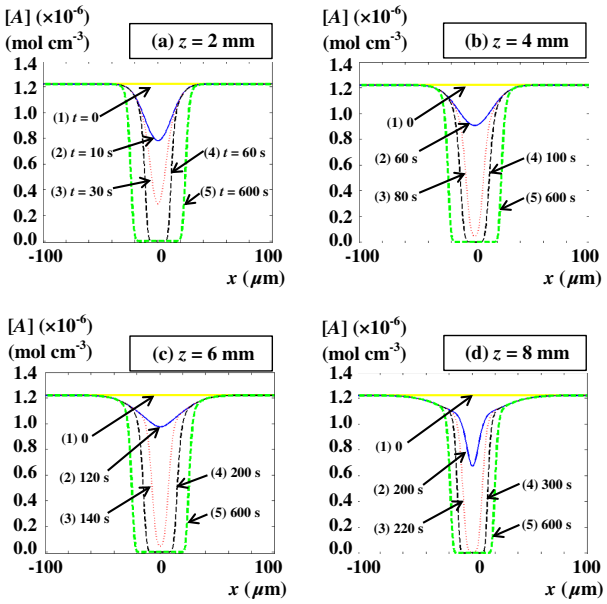

Fig. 7. Simulations of the spatial dye concentration distribution with a high initial concentration of $[A]_{high} = 12.2 \times 10^{-7}$ mol cm^{-3}, for four different x–z conditions: (a) $z = 2$ mm, (b) $z = 4$ mm, (c) $z = 6$ mm, and (d) $z = 8$ mm, and different exposure times are shown.

An example of the propagating light distribution obtained in a lower initial photosensitizer concentration case ($[A]_{low} = 1.22 \times 10^{-7}$ mol cm^{-3}) is shown in Fig. 8. As can be seen in Fig. 8, the changes in the beam intensity indicate that the SWW is formed gradually. Even though these are results for a low dye concentration case, weak nonlinear absorption and light diffraction can still be observed during the early exposure stages, i.e., when $t = 10$ s, especially deeper within the volume, i.e., when $z = 8$ mm. After some time, i.e., $15 \le t \le 20$ s, the index change increases, and the induced self-written channel can be observed to begin to restrain the diffraction of the writing beam. Finally, the Gaussian beam is self-trapped in the induced optical waveguide channel along the full length of the sample, i.e., $0 \le z \le 8$ mm. Recalling the simulation results presented in Fig. 2, we note that the experimental results exhibit the same SWW evolution qualitatively, supporting the validity of the model and procedure used.

Figure 9 shows the light propagations at different exposure times for the higher initial dye concentration ($[A]_{high} = 12.2 \times 10^{-7}$ mol cm^{-3}) case. The corresponding numerically simulated predictions were presented in Fig. 5. As predicted, the beam intensity shape follows the growth of the optical channel with the width remaining approximately constant in depth.

Experimental measurements were simultaneously made to determine the normalized transmittance [43–46] curves for the AA/PVA samples in both the lower and higher dye concentration cases. Some typical results are shown in Fig. 10. Fitting the experimental data, various parameter values appearing in the proposed model in Section 3 are extracted. The saturation values of the refractive index change in the phenomenological model, i.e., in Eq. (13), are chosen to be $\Delta n_s = 2.0 \times 10^{-3}$ (for the $[A]_{low}$ case) and 5.0×10^{-3} (for the $[A]_{high}$ case), respectively. The algorithm parameter values, e.g., the calculation window sizes (in x, z, t), and the step sizes and numbers remain the same as previously described in Section 4.

The estimated parameter values for the two cases are listed in Table 1. Mean square error (MSE) values are also provided to quantify the quality of the fitting. Based on the results in Table 1, it is worth noting that the values of molar absorptivity ε_D, quantum absorption efficiency of the dye Ψ_a and linear absorption coefficient α_L, estimated here, appear to be independent of the dye concentration, which supports the validity of the model used.

We note that the values of molar absorptivity, ε_D, estimated in Table 1, agree with results previously reported both in the area of holography and based on absorption spectrum measurements [43,44]. For example, according to previous fittings of holographic experimental measurements, the values of ε_D (molar absorptive) estimated for PB were in the range $0.316 \times 10^8 \le \varepsilon_D \le 0.537 \times 10^8$. Meanwhile, the value of ε_D calculated directly by measuring the absorption spectrum is 0.814×10^8 (see Fig. 2 and Table 2 presented in [44]). Because of material variability and experimental environment differences, e.g., the effects of temperature, humidity, and thermal variations on the materials, the observed variations

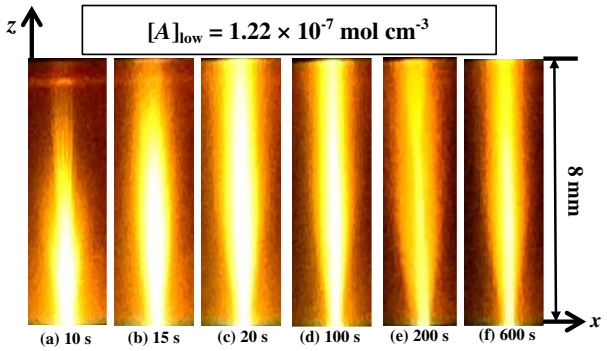

Fig. 8. Images of the propagating light distribution at different exposure times: t = (a) 10, (b) 15, (c) 20, (d) 100, (e) 200, and (f) 600 s, with the light ($\lambda = 532$ nm) incident on the AA/PVA sample containing a low dye concentration of the PB dye, $[A]_{low} = 1.22 \times 10^{-7}$ mol cm^{-3}.

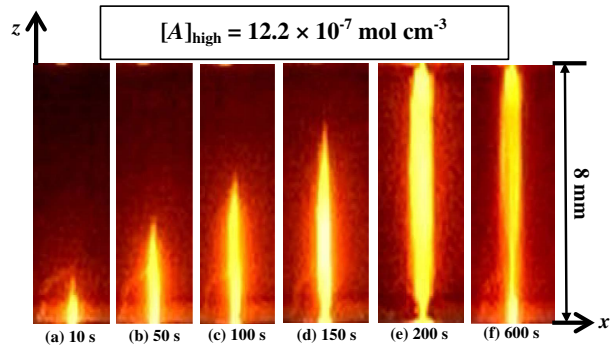

Fig. 9. Images of the propagating light distribution at different exposure times: t = (a) 10, (b) 50, (c) 100, (d) 150, (e) 200, and (f) 600 s, with the light ($\lambda = 532$ nm) incident on the AA/PVA sample containing a high dye concentration of PB dye, $[A]_{high} = 12.2 \times 10^{-7}$ mol cm^{-3}.

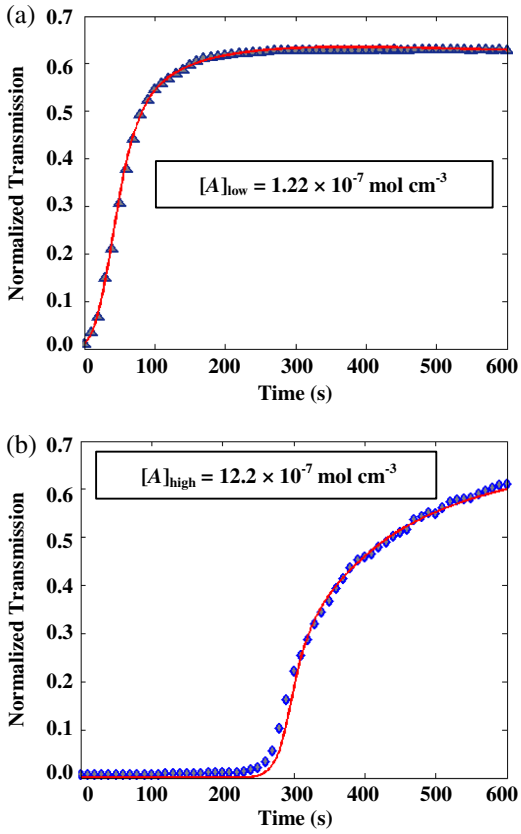

Fig. 10. Time varying normalized beam transmittance fits to the experimental data. The results are examined for the two initial dye concentration cases: (a) $[A]_{low} = 1.22 \times 10^{-7}$ mol cm^{-3} (red solid curve with blue triangles) and (b) $[A]_{high} = 12.2 \times 10^{-7}$ mol cm^{-3} (red solid curve with blue rhombuses).

in the estimated values of ε_D seem acceptable. Therefore, the average value of ε_D estimated here, i.e., $\varepsilon_D = 0.43 \times 10^8$, is reasonable and consistent.

We note that the differences observable in Figs. 10(a) and 10(b) between the experimental results and the fitted model predictions indicate that there are more complicated photophysical and photochemical processes taking place than those included in the model developed in Section 3. For example, the effects of the inhibition process, i.e., the effects of oxygen dissolved within the material, the excited dye recovery process, and the bleaching process should all be included if a more detailed study of the nonlinear photo-absorptive behavior in free radical photo-polymerization systems is to be performed [17,18,22,45,46]. However, such additional complexity will require the development of a more detailed theoretical model and a more complex numerical algorithm. For the model developed, the agreement is satisfactory and these absorptivity values extracted in this work are reasonable.

Examining Table 1, it can be seen that the linear absorption coefficient α_L estimated is predicted to a decrease from 0.55 to 0.45 cm^{-1} as the dye concentration increases. It is worth emphasizing that in this analysis the linear absorption coefficient α_L is considered to be very weak (i.e., solely describing losses because scattering), compared to the total light absorption, i.e., $\alpha = \alpha_L + \alpha_{NL}$. Recalling Eq. (11) in Section 3, it can be seen that the saturation values of α_{NL} obtained, are 5.6 cm^{-1} (for the $[A]_{low}$ case) and 48.8 cm^{-1} (for the $[A]_{high}$ case). The absolute percentage differences (PD, i.e., PD $= \Delta\alpha_L/\alpha \times 100\%$) between the linear absorption coefficient change $\Delta\alpha_L$, and the total light absorption α, are PD = 1.6% and 0.2% for the $[A]_{low}$ and $[A]_{high}$ cases, respectively. Thus, the values found are reasonable since α_L represents a weak and independent absorption effect. Once again the analysis provides consistent evidence supporting the validity of the model and procedures used.

6. CONCLUSIONS

In this paper, we began by reviewing the major photoreactions taking place during the photo-initiation process in a free radical photopolymer material. A set of rate equations was then derived, which governs the temporal and spatial photosensitizer concentration distribution during SWW formations. Assuming that the total attenuation parameter α, can be considered as the sum of the effect of a constant linear absorption coefficient α_L, and a nonlinear absorption coefficient α_{NL}, the time varying light energy loss in the material can be obtained assuming the dye concentration distribution as discussed in Section 2. Then combining the proposed linear and nonlinear absorption effects, with a phenomenological model [12–14] governing the index change induced in the material, a complete algorithm is implemented, which enables a more accurate and physical description of the evolution of SWWs formed in such photopolymer materials.

The predictions of the developed model are examined by performing simulations for two cases: (1) a lower initial photosensitizer concentration ($[A]_{low} = 1.22 \times 10^{-7}$ mol cm^{-3}) having a correspondingly weak nonlinear absorption, and (2) a higher initial photosensitizer concentration ($[A]_{high} = 12.2 \times 10^{-7}$ mol cm^{-3}) having a considerably higher nonlinear absorption.

The model is validated by performing a set of experiments under both dye concentration conditions in a standard free-radical photo-polymerization system, i.e., acrylamide/polyvinyl alcohol (AA/PVA). The time varying light distributions observed in these cases are, in general, in good qualitative agreement with the predictions of the model. Normalized

Table 1. Absorption Related Parameters Estimated from Fit to Experimental Transmittance Curves for Two Initial PB Dye Concentrations, in AA/PVA

$[A_o](\times 10^{-7})$ (mol cm^{-3})	$\varepsilon_D(\times 10^8)$ (cm^2 mol^{-1})	$\Psi_a(\times 10^{-8})$ (mol Einstein^{-1})	α_L (cm^{-1})	MSE$(\times 10^{-3})$
1.22	0.46	5.6	0.55	3.42
12.2	0.40	5.6	0.45	8.15
Average	**0.43**	**5.6**	**0.50**	—

transmittance measurements are also reported which provide information about the nonlinear photo-absorptive behavior during SWW formation. Absorption parameters are extracted by fitting the experimental results for both the lower and higher dye concentration cases. The results are in good quantitative agreement with previous results in the literature [43,44].

Much work remains to be done. A complete kinetic model must be developed describing the full photo-polymerization process and taking into account all the effects taking place while the index change is induced, e.g., nonlocal polymer chain growth and material transport [47,48]. In that case, given the time varying material component concentrations, the refractive index can be calculated using the Lorentz–Lorenz formula [15,47]. Access to such a model would allow the use of such effects to couple optical fiber [49,50] and polymer microtip fabrication [51,52], to be studied quantitatively and optimized.

Irish Research Council for Science, Engineering and Technology (IRCSET); Science Foundation Ireland (SFI).

H. Li is supported by a University College Dublin-China Scholarship Council joint scholarship. Y. Qi is supported by the EU ERASMUS Mundus fund. R. Malallah is supported by the Iraqi Ministry of Higher Education and Scientific Research. The authors would also like to acknowledge the support of the Irish Research Council for Science, Engineering and Technology (IRCSET), Enterprise Ireland and Science Foundation Ireland (SFI) under the National Development Plan (NDP).

REFERENCES

1. A. S. Kewitsch and A. Yariv, "Self-focusing and self-trapping of optical beams upon photopolymerization," Opt. Lett. **21**, 24–26 (1996).
2. M. Kagami, T. Yamashita, and H. Ito, "Light-induced self-written three-dimensional optical waveguide," Appl. Phys. Lett. **79**, 1079–1081 (2001).
3. R. Bachelot, C. Ecoffet, D. Deloeil, P. Royer, and D. J. Lougnot, "Integration of micrometer-sized polymer elements at the end of optical fibers by free-radical photopolymerization," Appl. Opt. **40**, 5860–5871 (2001).
4. S. Shoji, S. Kawata, A. A. Sukhorukov, and Y. Kivshar, "Self-written waveguides in photopolymerizable regins," Opt. Lett. **27**, 185–187 (2002).
5. K. Dorkenoo, O. Crégut, L. Mager, F. Gillot, C. Carre, and A. Fort, "Quasi-solitonic behaviour of self-written waveguides created by photopolymerization," Opt. Lett. **27**, 1782–1784 (2002).
6. C. P. Jisha, V. C. Kishore, B. M. John, V. C. Kuriakose, K. Porsezian, and C. S. Kartha, "Self-written waveguide in methylene blue sensitized poly(vinyl alcohol)/acrylamide photopolymer material," Appl. Opt. **47**, 6502–6507 (2008).
7. E. Tolstik, O. Kashin, V. Matusevich, and R. Kowarschik, "Broadening of the light self-trapping due to thermal defocusing in PQ-PMMA polymeric layers," Opt. Express **19**, 2739–2747 (2011).
8. E. Tolstik, O. Romanov, V. Matusevich, A. Tolstik, and R. Kowarschik, "Formation of self-trapping waveguides in bulk PMMA media doped with Phenanthrenequinone," Opt. Express **22**, 3228–3233 (2014).
9. J. Missinne, S. Beri, M. Dash, S. K. Samal, P. Dubruel, J. Watté, and G. V. Steenberge, "Curing kinetics of step-index and graded-index single mode polymer self-written waveguides," Opt. Express **4**, 1324–1335 (2014).
10. H. Li, Y. Qi, J. P. Ryle, and J. T. Sheridan, "Self-written waveguides in a dry Acrylamide/polyvinyl alcohol photopolymer material," Appl. Opt. **53**, 8086–8094 (2014).
11. R. Y. Chiao, E. Garmire, and C. H. Townes, "Self-trapping of optical beams," Phys. Rev. Lett. **13**, 479–482 (1964).
12. A. S. Kewitsch and A. Yariv, "Nonlinear optical properties of photoresists for projection lithography," Appl. Phys. Lett. **68**, 455–457 (1996).
13. T. M. Monro, L. Poladian, and C. M. Sterke, "Analysis of self-written waveguides in photopolymers and photosensitive materials," Phys. Rev. E **57**, 1104–1113 (1998).
14. T. M. Monro, D. Moss, M. Bazylenko, C. M. Sterke, and L. Poladian, "Observation of self-trapping of light in a self-written channel in a photosensitive glass," Phys. Rev. Lett. **80**, 4072–4075 (1998).
15. O. Kashin, E. Tolstik, V. Matusevich, and R. Kowarschik, "Numerical investigation of the (1 + 1) D self-trapping of laser beams in polymeric films based on polymethylmethacrylate and phenanthrenequinone," J. Opt. Soc. Am. B **26**, 2152–2156 (2009).
16. A. M. Kashin and T. M. Monro, "Exploration of self-writing and photosensitivity inion-exchanged waveguides," J. Opt. Soc. Am. B **20**, 1317–1325 (2003).
17. M. R. Gleeson, J. V. Kelly, C. E. Close, F. T. O'Neill, and J. T. Sheridan, "Effects of absorption and inhibition during grating formation in photopolymer materials," J. Opt. Soc. Am. B **23**, 2079–2088 (2006).
18. M. R. Gleeson, S. Liu, S. O'Duill, and J. T. Sheridan, "Examination of the photoinitiation processes in photopolymer materials," J. Appl. Phys. **104**, 064917 (2008).
19. Y. Qi, H. Li, J. P. Fouassier, J. A. Lalevée, and J. T. Sheridan, "Comparison of a new photosensitizer with erythrosine B in an AA/PVA based photopolymer material," Appl. Opt. **53**, 1052–1062 (2014).
20. H. Li, Y. Qi, J. Guo, and J. T. Sheridan, "Analysis of the absorptive behavior of photopolymer materials. Part I. Theoretical modeling," J. Mod. Opt. **62**, 145–156 (2015).
21. H. Li, Y. Qi, and J. T. Sheridan, "Three-dimensional extended nonlocal photo-polymerization driven diffusion model. Part I. Absorption," J. Opt. Soc. Am. B **31**, 2638–2647 (2014).
22. M. R. Gleeson, S. Liu, J. Guo, and J. T. Sheridan, "Non-local photopolymerization kinetics including multiple termination mechanisms and dark reactions: Part III. Primary radical generation and inhibition," J. Opt. Soc. Am. B **27**, 1804–1812 (2010).
23. J. B. Birk, *Organic Molecular Photophysicals* (Wiley, 1975).
24. A. Gilbert and J. Baggott, *Essentials of Molecular Photochemistry* (Blackwell Scientific, 1991).
25. A. E. Siegman, *Lasers* (University Science, 1986).
26. C. Tsao, *Optical Fibre Waveguide Analysis* (Oxford University, 1992).
27. D. Engin, A. S. Kewitsch, and A. Yariv, "Holographic characterization of chain photopolymerization," J. Opt. Soc. Am. B **16**, 1213–1219 (1999).
28. G. P. Agrawal, *Nonlinear Fiber Optics*, 7th ed. (Academic, 2000).
29. E. H. Twizell, A. G. Bratsos, and J. C. Newby, "A finite-difference method for solving the cubic Schrödinger equation," Math. Comput. Simulat. **43**, 67–75 (1997).
30. D. M. Sullivan, *Electromagnetic Simulation using the FDTD Method* (IEEE, 2000).
31. J. Francés, C. Neipp, M. Pérez-Molina, and A. Beléndez, "Rigorous interference and diffraction analysis of diffractive optic elements using the finite-difference time-domain method," Comput. Phys. Commun. **181**, 1963–1973 (2010).
32. J. A. C. Weideman and B. M. Herbst, "Split-step methods for the solution of the nonlinear Schrödinger equation," SIAM J. Numer. Anal. **23**, 485–507 (1986).
33. D. Dockery and J. R. Kuttler, "An improved impedance-boundary algorithm for Fourier split-step solutions of the parabolic wave equation," IEEE Trans. Antennas Propag. **44**, 1592–1599 (1996).
34. O. V. Sinkin, R. Holzlöhner, J. Zweck, and C. R. Menyuk, "Optimization of the split-step Fourier method in modeling optical-fiber communications systems," J. Lightwave Technol. **21**, 61–68 (2003).
35. B. Fornberg and T. A. Driscoll, "A fast spectral algorithm for nonlinear wave equations with linear dispersion," J. Comput. Phys. **155**, 456–467 (1999).

36. E. B. Dynkin, "Calculation of the coefficients in the Campbell-Hausdorff formula," Doklady Akad. Nauk SSSR (NS) **57**, 323–326 (1947).
37. L. Mandel and E. Wolf, *Optical Coherence and Quantum Optics* (Cambridge University, 1995).
38. P. Duhamel and M. Vetterli, "Fast Fourier transforms: a tutorial review and a state of the art," Signal Process. **19**, 259–299 (1990).
39. S. Liu, C. Guo, and J. T. Sheridan, "A review of optical image encryption techniques," Opt. Laser Technol. **57**, 327–342 (2014).
40. J. A. Fleck, Jr., J. R. Morris, and M. D. Feit, "Time-dependent propagation of high energy laser beams through the atmosphere," Appl. Phys. **10**, 129–160 (1976).
41. T. M. Monro, P. D. Miller, L. Poladian, and C. M. Sterke, "Self-similar evolution of self-written waveguides," Opt. Lett. **23**, 268–270 (1998).
42. H. Li, Y. Qi, E. Tolstik, J. Guo, and J. T. Sheridan, "Analysis of the absorptive behavior of photopolymer materials. Part II. Experimental validation," J. Mod. Opt. **62**, 157–167 (2015).
43. Y. Qi, H. Li, J. Guo, M. R. Gleeson, and J. T. Sheridan, "Material response of photopolymer containing four different photosensitizers," Opt. Commun. **320**, 114–124 (2014).
44. Y. Qi, M. R. Gleeson, J. Guo, S. Gallego, and J. T. Sheridan, "Quantitative comparison of five different photosensitizers for use in a photopolymer," Phys. Res. Int. **2012**, 975948 (2012).
45. M. Hocine, N. Fressengeas, G. Kugel, C. Carré, D. J. Lougnot, R. Bachelot, and P. Royer, "Modeling the growth of a polymer microtip on an optical fiber end," J. Opt. Soc. Am. B **23**, 611–620 (2006).
46. O. Soppera, S. Jradi, and D. J. Lougnot, "Photopolymerization with microscale resolution: influence of the physic-chemical and photonic parameters," J. Polym. Sci., Part A Polym. Chem. **46**, 3783–3794 (2008).
47. H. Li, Y. Qi, and J. T. Sheridan, "Three-dimensional extended nonlocal photo-polymerization driven diffusion model. Part II. Photopolymerization and model development," J. Opt. Soc. Am. B **31**, 2648–2656 (2014).
48. A. Ibrahim, X. Allonas, C. Ley, B. E. Fouhaili, and C. Carré, "Photocyclic initiating system for free radical photopolymerization studied through holographic recording," J. Photopolym. Sci. Tech. **27**, 517–523 (2014).
49. R. Bachelot, A. Fares, R. Fikri, D. Barchiesi, G. Lerondel, and P. Royer, "Coupling semiconductor lasers into single-mode optical fibers by use of tips grown by photopolymerization," Opt. Lett. **29**, 1971–1973 (2004).
50. C. Pang, F. Gesuele, A. Bruyant, S. Blaize, G. Lérondel, and P. Royer, "Enhanced light coupling in sub-wavelength single-mode silicon on insulator waveguides," Opt. Express **17**, 6939–6945 (2009).
51. L. Xiao, W. Jin, M. S. Demokan, H. L. Ho, H. Y. Tam, J. Ju, and J. Yu, "Photopolymer microtips for efficient light coupling between single-mode fibers and photonic crystal fibers," Opt. Lett. **31**, 1791–1793 (2006).
52. S. Jradi, O. Soppera, and D. J. Lougnot, "Fabrication of polymer waveguides between two optical fibers using spatially controlled light-induced polymerization," Appl. Opt. **47**, 3987–3993 (2008).